ARHGAP18: A Flow-Responsive Gene That Regulates Endothelial Cell Alignment and Protects Against Atherosclerosis

Angelina J. Lay, PhD; Paul R. Coleman, PhD;* Ann Formaz-Preston, MD, MSc;* Ka Ka Ting, PhD; Ben Roediger, PhD; Wolfgang Weninger, MD, PhD; Martin A. Schwartz, PhD; Mathew A. Vadas, MD, PhD; Jennifer R. Gamble, PhD

Background—Vascular endothelial cell (EC) alignment in the direction of flow is an adaptive response that protects against aortic diseases, such as atherosclerosis. The Rho GTPases are known to regulate this alignment. Herein, we analyze the effect of ARHGAP18 on the regulation of EC alignment and examine the effect of ARHGAP18 deficiency on the development of atherosclerosis in mice.

Methods and Results—We used in vitro analysis of ECs under flow conditions together with apolipoprotein E$^{-/-}$ Arhgap18$^{-/-}$ double-mutant mice to study the function of ARHGAP18 in a high-fat diet–induced model of atherosclerosis. Depletion of ARHGAP18 inhibited the alignment of ECs in the direction of flow and promoted inflammatory phenotype, as evidenced by disrupted junctions and increased expression of nuclear factor-κB and intercellular adhesion molecule-1 and decreased endothelial nitric oxide synthase. Mice with double deletion in ARHGAP18 and apolipoprotein E and fed a high-fat diet show early onset of atherosclerosis, with lesions developing in atheroprotective regions.

Conclusions—ARHGAP18 is a protective gene that maintains EC alignments in the direction of flow. Deletion of ARHGAP18 led to loss of EC ability to align and promoted atherosclerosis development. (*J Am Heart Assoc*. 2019;8:e010057. DOI: 10.1161/JAHA.118.010057.)

Key Words: animal model • ARHGAP18 • endothelial cell • atherosclerosis

The vascular bed is constantly exposed to hemodynamic shear stress imposed by the flowing blood. The endothelial cells (ECs) that line the vessels are the key cells that are affected by this stress, with the greatest force occurring at the cell-cell junctions.[1] In a process known as mechanotransduction, the ECs have the ability to sense the fluid shear stress, the frictional force from blood flow, and convert this into biochemical signals that affect the morphology and function of the cells.[1]

Atherosclerosis, a chronic inflammatory disease characterised by arterial wall thickening, is a major cause of morbidity and death in developed countries.[2,3] Although atherosclerosis development involves the contribution of many cell types to plaque development, changes to the endothelium are recognized

as one of the initial events and result in the progressive accumulation of immune cells within the region and a state of chronic inflammation.[4] Atherosclerotic plaques preferentially develop at branched or bifurcated arterial sites.[5] These athero-prone sites are characterized by disturbed blood flow, in which flow patterns are complex and lack direction and hemodynamic shear stress is low.[6,7] In contrast, the athero-protected regions are areas of high shear laminar flow and are generally resistant to atherosclerosis development.[8] In these laminar flow areas, ECs align in the direction of flow, and this alignment is considered an adaptive protective response to the stress of high blood flow.[9] The alignment promotes the expression of anti-inflammatory or cytoprotective genes, such as endothelial nitric oxide synthase (eNOS),[10] and the transcription factors KLF2 and

<div style="border: 2px solid red; padding: 1em;">

Clinical Perspective

What Is New?

- ARHGAP18 is a key regulator of endothelial cell alignment in response to high shear laminar flow.
- Ablation of ARHGAP18 leads to loss of atheroprotection in areas that normally are low risk for atherosclerosis.
- ARHGAP18 is a novel vascular protective gene.

What Are the Clinical Implications?

- Restoration or enhancement of ARHGAP18 activity, or components of its downstream pathway, may offer therapeutic potential.
- Changes in ARHGAP18 levels or activity may predispose to atherosclerosis development.

</div>

KLF4 (Kruppel-like factors).[11–13] In contrast, in regions of disturbed flow, the ECs are disorganized, fail to align in the direction of flow, and lack mature adherens junctions.[14] These are regions that show altered patterns of inflammatory gene expression, particularly increased expression of proinflammatory genes, such as intercellular adhesion molecule 1 (ICAM-1), and the transcription factor nuclear factor-κB (NF-κB). These patterns of gene expressions dictate the site-specific inflammatory phenotype of ECs and ultimately affect disease initiation and progression.[9]

Members of the small Rho GTP-binding proteins are important molecular switches for the regulation of many cellular processes, including cell shape. In particular, Rho activity is critical in EC alignment in response to shear stress. RhoA activity is upregulated in the initial response to laminar flow, but its downregulation is essential to the alignment of the ECs in the direction of flow and in the atheroprotection.[15] The activity of the GTPases is regulated by 3 mediators: guanine nucleotide exchange factors, which activate GTPases; GTPase-activating proteins (GAPs), which deactivate the activity; and guanine nucleotide–dissociation inhibitors, which sequestrate the GTPase.[16] The regulation of Rho GTPases by GAP and guanine nucleotide exchange factor exhibits cell- and function-specific selectivity.[17] One such RhoGAP, ARHGAP18, is highly expressed in ECs, and we have shown previously that it has both GAP-dependent and GAP-independent roles, consistent with that seen for its homologue, Conundrum, in *Drosophila*.[18] ARHGAP18 (aka, *SENEX*) is involved in promoting EC senescence in a GAP-independent manner, and its expression is essential for EC survival under stress.[19] Interestingly, ARHGAP18-induced senescent ECs have anti-inflammatory properties[19,20] through caveolae upregulation.[21] ARHGAP18 also is involved in the stabilization of EC cell junctions, it limits angiogenic sprouting, and it regulates the

actin cytoskeleton in a RhoC-dependent manner.[22] In contrast, ARHGAP18 in non-ECs shows RhoA activity.[23] Most recently, we have shown that ARHGAP18 is also important in smooth muscle cell phenotype, inhibiting the contractile-to-synthetic conversion, maintaining the associated anti-inflammatory phenotype, and limiting thoracic aortic aneurysm formation.[24] Thus, we suggest that ARHGAP18 is essential in the vasculature to maintain its anti-inflammatory state.

Cell junctional regulation and the actin cytoskeletal components are critical in the mechanotransduction signalling in ECs to mediate the anti-inflammatory aligned shape change under laminar flow.[25,26] Thus, we hypothesized that ARHGAP18 may be a key negative regulator of the Rho GTPase pathway involved in the protective alignment of ECs in response to flow. To test this hypothesis, we investigated the effect of ARHGAP18 deletion on the endothelial response to flow and its consequence on the development of high-fat diet (HFD)–induced atherosclerosis.

Materials and Methods

The data, analytic methods, and study materials will be made available to other researchers for purposes of reproducing the results or replicating the procedure. The material is held at the Centenary Institute (Newtown, Australia).

Generation of ARHGAP18 Knockout Mouse

Mutant mice carrying a targeted deletion of *Arhgap18* (*SENEX*) were generated using gene-trapping approach, as is outlined in Figure S1. The targeted knockout allele ES cells from International Gene Trapping Consortium/Knockout Mouse Project were microinjected into fertilized C57B/L6 oocytes for chimera production in JAX Laboratory. The targeted allele was generated using a 6.9-kb trapping cassette flanked by a 5′ splice acceptor sequence and a 3′ polyadenylation sequence. Through efficient splicing to the reporter cassette, a constitutive null mutation in the ARHGAP18 gene was generated, resulting in global *Arhgap18* knockout. Mice carrying targeted allele were identified by polymerase chain reaction (PCR) using specific primers and confirmed by sequence analysis. Homozygous ARHGAP18 ($Arhgap18^{-/-}$) strain was bred with homozygous apolipoprotein E ($ApoE^{-/-}$) strain to generate the double-knockout (DKO) strain ($ApoE^{-/-}/Arhgap18^{-/-}$) in the F2 generation.

In Vitro Shear Flow Experiment

The use of discarded human umbilical cords, for the isolation of ECs, was approved by the Sydney Local Health District Human Ethics Committee, approval (X16-0225) with donor informed consent. Human umbilical vein ECs (HUVECs) were isolated and maintained in 5% CO_2 incubator, according to the established

method.[27] HUVECs were used at passage 1 to 3 for all experiments. Fifty thousand cells were cultured on IBIDI Y-shaped slides for 24 hours to allow attachment, then either kept as static controls or exposed to laminar flow at 20 dynes/cm^2 using IBIDI pump system (IBIDI GmbH, Germany). Gene expression studies were performed using RNA samples from HUVECs cultured on straight IBIDI slides and then subjected to laminar (20 dynes/cm^2) or oscillating/disturbed (2 dynes/cm^2 per 1 Hz) flow. For immunofluorescence stain, slides were fixed for 15 minutes with 4% paraformaldehyde and permeabilized for 10 minutes with 0.1% Triton X-100 in PBS, followed by 2-hour blocking with 2% BSA before probing with various antibodies. Primary antibodies and concentrations used were: mouse monoclonal anti-ARHGAP18 (clone 2A3-F, in house, 5 μg/mL), rhodamine phalloidin (catalog No. R415, Life Technologies), mouse monoclonal anti-acetylated tubulin (catalog No. T7451, Sigma Aldrich), rabbit monoclonal anti–NF-κB p65 (catalog No. C22B4, Cell Signaling), rabbit monoclonal anti–vascular endothelial cadherin (anti-VE-cadherin) (catalog No. D87F2, Cell Signaling), mouse anti-eNOS (catalog No. 610297, BD), and rabbit anti–ICAM-1 (catalog No. 4915, Cell Signaling).

Mice and HFD Treatment

ApoE$^{-/-}$/*Arhgap18*$^{-/-}$ or ApoE$^{-/-}$ control mice were maintained under standard husbandry conditions at the Centenary Institute Animal Facility. All experimental procedures were performed in accordance with the Sydney Local Health District Animal Welfare Committee approval (2013-060). For HFD model, male mice at 8 to 10 weeks old were fed either standard HFD, consisting of 45% kcal cholesterol, 35% CHO (Chinese hamster ovary cells), and 20% kcal protein (D12451; Research Diets, New Brunswick, NJ) supplemented with 5% fructose in the drinking water, or normal diet for 4 to 20 weeks. Water and food were provided ad libitum. Body weights were monitored weekly. At specified time points (4, 8, and 20 weeks), mice were euthanized.

Oil Red O Stain

Atherosclerotic plaques were detected using Oil Red O stain for lipid content. Briefly, the aortic tree was dissected between the ascending aorta and the iliac bifurcation. After carefully removing the surrounding adipose tissue, a longitudinal incision was made along the trunk, with all the arches, including the innominate, right cephalic, and right carotid, to expose the lumen side. The opened aortic arches/tree was then mounted between 2 glass slides and fixed overnight in 10% buffered formalin solution. Samples was rinsed in isopropanol for 10 minutes before being stained with 5% of Oil red O dissolved in isopropanol for 1 hour, followed by 2 washes in PBS. Atherosclerotic plaques were imaged using Leica stereomicroscope (model M205FA) and quantitated using ImageJ software.

Histological Analysis of Atherosclerotic Plaque

Tissues were fixed in formalin overnight, followed by paraffin embedded. A serial of 4- to 5-μm thick sections was obtained from the proximal aortas and stained with hematoxylin and eosin. Hematoxylin and eosin–stained sections of atherosclerotic plaque from area of similar depth were used for comparison of plaque size or for the determination of cellular composition by immunohistochemical or immunofluorescence stains. Plaque sizes were determined by measuring the total plaque area in the intima using ImageJ software. All measurements represent the total area from 10 mice.

Lipid Chemistry

Analysis for total triglyceride and total cholesterol, including low- and high-density lipoproteins, was performed by the Sydney Local Health District pathology service. All plasma samples were collected from mice after an overnight fasting.

En Face Immunofluorescence Stain of Aortic Tree

Male mice, aged 8 to 10 weeks, were euthanized and pressure perfused with saline through the left ventricle, followed by perfusion with 5 mL of chilled 4% paraformaldehyde solution. The aortic tree was carefully dissected and opened longitudinally to expose the lumen. The tree was then sandwiched between 2 glass slides and fixed in 4% paraformaldehyde for another 2 hours on ice, followed by an overnight blocking with PBS containing 1% BSA. All primary antibodies were prepared in PBS containing 1% BSA and 5% normal serum. The following primary antibodies were used: rat anti-mouse VE-cadherin or CD144 (1:200), rabbit polyclonal antibody to ICAM-1 (1:400), rabbit monoclonal antibody to NF-κB p65 (1:400), mouse anti-eNOS (1:200), and in-house mouse monoclonal antibody to ARHGAP18 (1:50). Samples were incubated in primary antibody for 2 days. For mouse antibodies (eNOS and ARHGAP18), further blocking step with Mouse On Mouse blocking reagents was added to block endogenous mouse IgG stain before primary antibody incubation. Samples were washed with PBS/Tween 20 for 2 hours (12×10 minute washes). All secondary antibodies were used at 1:2000 dilution, incubated for 2 hours at room temperature, and washed for 2 hours before staining with DAPI (1:50) for 10 minutes. Aortas with lumen facing up were mounted and coverslipped using Prolong Gold. Images were captured at ×63 using confocal microscope (Leica TCS SP5) using an HCX PL APO Lbd Bl 63×/1.40 to 0.60 numerical aperture objective. All images for p65, eNOS, ICAM, and ARHGAP18 were captured at the EC layer, as identified by VE-cadherin staining.

Small-Interfering RNA Method

For ARHGAP18 knockdown, HUVECs were transfected with either stealth small-interfering RNA (siRNA) control (low GC content, 5 nmol/L) or 2 stealth siRNAs (HSS132562, HSS190252; 5 nmol/L; Life Technologies) using Lipofectamine RNAiMAX (Life Technologies), as previously described.[22]

Quantitative Reverse Transcription–PCR

RNAs were isolated from tissue or cell culture homogenate using TRIzol (Life Technologies) reagent, according to manufacturer's protocol. The RNA was treated with DNase I (Sigma-Aldrich) and reverse transcribed using the High Capacity cDNA Synthesis Kit (Life Technologies). All transcription reactions were performed in triplicate with 2.5 ng of equivalent cDNA, 0.2 μmol/L of forward and reverse primer, and 1× SYBR green jumpstart mix (Sigma-Aldrich). Reactions were run in a Rotor-Gene 3000 PCR machine (Corbett, Qiagen) using a 4-step PCR cycling protocol consisting of 95°C for 10 minutes, 40 cycles of 95°C for 15 seconds, 62°C for 40 seconds, 72°C for 40 seconds, and 78°C for 15 seconds, and acquisition to the FAM channel. Melt curve analysis was performed at the end of the PCR cycling to confirm the absence of nonspecific products. Relative gene expression changes were calculated using the 2-ΔΔCT method.[28] ARHGAP18 primers were: forward, CGAGCAAGCACTCAATCA-GAAAGAGAG; reverse, GCTGTCAATGGAACGCAAAAAAGAC-CAG.

Western Blot Analysis

Total cell lysates were prepared from HUVECs exposed to various experimental conditions. Equal amounts of total proteins (8 μg) were loaded and separated on 4% to 12% NuPAGE gradient gel (Life Technologies), transferred to polyvinylidene difluoride membrane, and detected with enhanced chemiluminescence substrate (Pierce), as per the manufacturer's instructions. Vascular cell adhesion molecule 1 (catalog No. ab134047, Abcam), eNOS (catalog No. 610297, BD Biosciences), and ARHGAP18 clone 2A3-F3 (in house) were used at 1:500 to 1:1000, and actin–horseradish peroxidase was used at 1:10,000 dilution in PBS/Tween 20 containing 1% BSA.

Statistical Analysis

All calculated values represent mean±SD. Statistical significance was determined by unpaired 2-tailed Student t test to compare means. Mean differences with $P<0.05$ was considered statistically significant.

Results

ARHGAP18 Is Required for EC Alignment

To determine whether ARHGAP18 is regulated by flow, its expression was investigated under laminar and disturbed flow. Using Y-shaped IBIDI slides, we investigated the expression of ARHGAP18 at points subjected to high shear stress laminar flow and those subjected to disturbed flow, at the points of bifurcations (Figure 1Ai). ECs subjected to laminar flow aligned in the direction of flow (Figure 1Aii–v). In contrast, cells under disturbed flow not only showed high protein expression of ARHGAP18 but also failed to align under these conditions, as reported previously[20] (Figure 1Avi–ix). Quantification of protein expression, on the basis of pixel intensity (16.6±2.14 versus 23.4±2.29), confirmed this (Figure 1Ax). Consistent with this, cultured HUVECs (ECs) exposed to 72 hours of steady high shear, laminar flow (20 dynes/cm^2) showed low levels of ARHGAP18 mRNA, whereas those under oscillating/disturbed (2 dynes/cm^2 per 1 Hz) or static conditions had higher levels (laminar, 0.25±0.07; disturbed, 0.94±0.26; and static, 1±0.3) (Figure 1B). Furthermore, the protein levels of ARHGAP18 were significantly increased under static conditions compared with cells under high shear laminar flow (Figure S2A).

Flow regulation of ARHGAP18 was seen also in vivo, where en face staining for ARHGAP18 expression in the aorta of mice showed decreased expression in the high shear laminar flow regions of the thoracic aorta compared with that seen in the disturbed flow regions of the aortic arch (0.6±0.1-fold change) (Figure 1Ci–iii). In addition, there was enhanced expression in the inner curvature of the aorta, compared with levels seen in the outer curvature (Figure 1Civ, v), consistent with the flow being more disturbed in the inner compared with the outer curvature in the arch region.[6]

To determine whether ARHGAP18 is crucial for EC alignment, we depleted ARHGAP18 using siRNAs, which we have previously characterized[22] and which resulted in knockdown of >90% of ARHGAP18 protein (Figure S2B). ECs with depleted levels of ARHGAP18 cultured under normal static conditions (high serum levels and growth factors) remained viable, and there was no change in morphology compared with cells treated with control siRNA (Figure 2Ai and ii). Cells were subjected to steady high shear, laminar flow (20 dynes/cm^2). Control siRNA treated cells aligned in the direction of flow (Figure 2Aiii). However, ARHGAP18 deletion ablated the capacity of the cells to uniformly align in the direction of high shear laminar flow (Figure 2Aiv). Staining for actin fibers showed that *Arhgap18*-depleted ECs lacked uniform orientation of the actin stress fibers in the direction of the flow compared with control ECs, which had unidirectional, well-
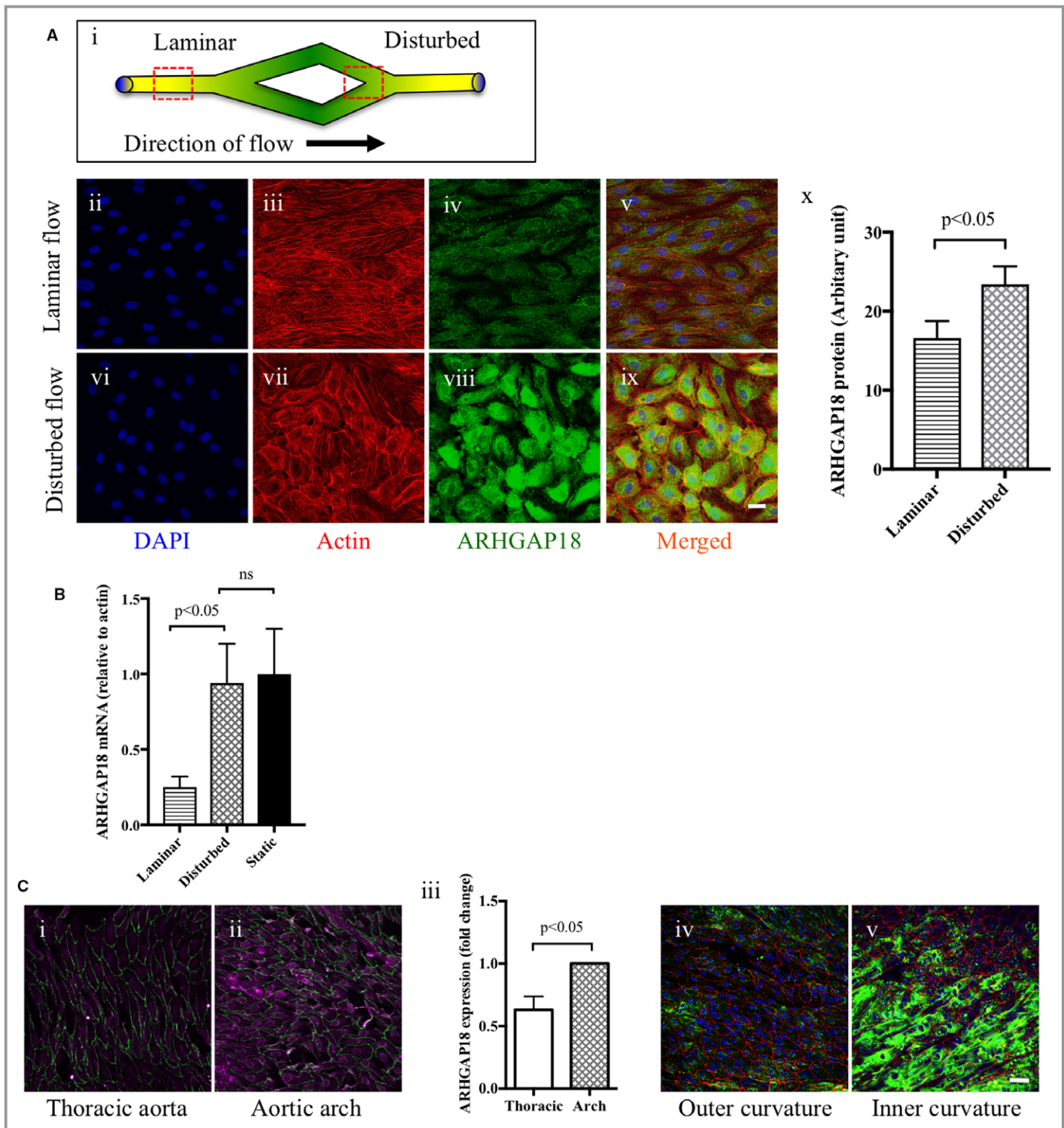
Figure 1. ARHGAP18 is flow responsive. (**A**) In vitro analysis of ARHGAP18 protein expression under different flow conditions. Schematic Y-shaped IBIDI flow system showing area of laminar and disturbed flow (red boxes) with direction of flow as indicated (i). Staining for ARHGAP18 (green), F-actin (red), and 4',6-diamidino-2-phenylindole (DAPI) for nuclei (blue) in these areas (ii-ix). Images are representative of 4 experiments, which are quantified (x). Bar=25 μm. (**B**) Analysis of mRNA during high shear laminar flow and disturbed flow after 72 hours of flow. (**C**) En face staining of ARHGAP18 expression (magenta), with costaining for VE-cadherin (green) in area of high shear flow in the thoracic aorta (i) compared with the disturbed flow area of the aortic arch (ii). (iii) Quantification of mean pixel intensity for ARHGAP18 stain and expressed as fold change. Expression of ARHGAP18 in the outer curvature (iv) and the inner curvature (v) of the aorta. Representative image from 3 mice. Bar=25 μm. Ns indicates not significant.
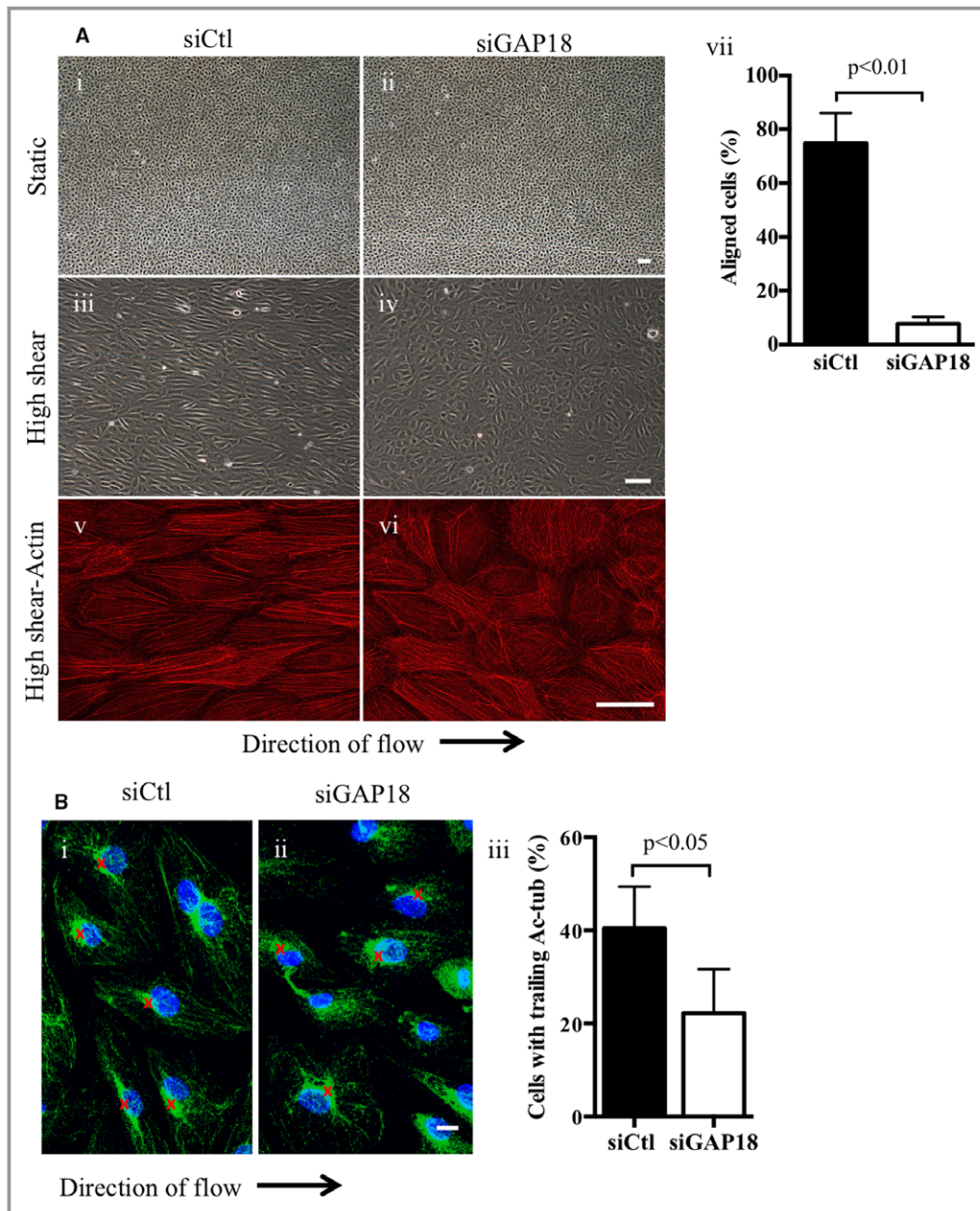
Figure 2. Endothelial cell (EC) alignment in response to flow–required ARHGAP18. (**A**) Morphological characteristics of control small–interfering RNA (siCtl; i, iii, and v) or small–interfering ARHGAP18 (siGAP18)–treated ECs (ii, iv, and vi) under static condition (i and ii) and under high shear flow (iii–vi) with F-actin staining (red) (v and vi). Direction of flow as indicated. Representative of 5 independent experiments (vii). Quantification of cellular alignment determined by counting the number of cells with actin stress fibers that were parallel to the direction of the major axis of cells. Approximately 900 to 1000 cells were counted, from 3 to 4 biological replicates (74.8±11.26 vs 7.73±2.5, siCtl versus siGAP18). Bar=25 μm. (**B**) The number of cells showing microtubule–organizing center aligned behind the nucleus (blue) in the direction of flow, as determined by acetylated tubulin stain (green) in siCtl cells (i) or siGAP18-treated cells (ii), 4 hours after exposure to high shear flow. (iii) Cells with trailing acetylated tubulin were counted from 5 images taken per group from 5 independent experiments (40.4±8.96 vs 22.2±9.42 siCtl versus siGAP18). Bar=10 μm.

organized actin stress fibers (Figure 2Av and vi). Quantification of the percentage of cells that showed actin alignment in the direction of flow confirmed this (74.8±11.26 versus 7.73±2.5) (Figure 2Avii).[29]

The depletion of ARHGAP18 affected the early response to flow, a time when the actin cytoskeleton is being remodeled and the Rho GTP activity is reduced.[30] This was measured by the movement of the microtubule–organizing center,

downstream of the nucleus relative to the direction of flow.[31] Consistent with the reported literature, microtubule–organizing center, as marked by acetylated tubulin stain, is observed in ≈40% of the small-interfering control–treated ECs (Figure 2Bi, red cross). In contrast, depletion of ARHGAP18 significantly reduced the ability of ECs to polarize microtubule-organizing center, with only ≈20% of cells having trailing acetylated tubulin (40.4±8.96 versus 22.2±9.42) (Figure 2Bii, iii).

We have previously reported the generation of ARHGAP18-deficient mice (*Arhgap18*$^{-/-}$) that are phenotypically normal and age normally.[22] These mutant mice were generated from targeted knockout allele ES cells from International Gene Trapping Consortium/Knockout Mouse Project (Figure S1A through S1D). We examined EC alignment in wild-type (WT) and *Arhgap18*$^{-/-}$ mice under basal conditions. En face staining of the thoracic aorta for the EC-specific cadherin, VE-cadherin, showed its localization to cell-cell junctions. In WT mice, the ECs displayed the characteristic elongated phenotype (Figure 3i, iii, v). In contrast, in *Arhgap18*$^{-/-}$ mice, the ECs failed to align in the direction of flow (Figure 3ii, iv, vi), showing a predominantly cuboidal shape, with prominent wide zipperlike appearance of VE-cadherin at cell-cell junctions, indicative of disrupted junctions[32] (Figure 3vi, arrows). Measurement of cell circularity (0.28±0.02 versus 0.44 ±0.04) (Figure 3vii) confirmed the morphological changes, suggesting that ARHGAP18 is important for the alignment of ECs in the direction of flow.

Although *Arhgap18*$^{-/-}$ mice are viable and reproduce normally, ECs isolated from the *Arhgap18*$^{-/-}$ aortic vessels were not sustainable in culture and had limited survival beyond the initial passages, compared with ECs derived from aorta of WT littermates (data not shown). This is consistent with our previous findings, in which we showed that knockdown of ARHGAP18 in ECs cultured under suboptimal conditions or in the presence of high tumor necrosis factor-α levels rendered them proapoptotic.[19] Our previous findings also showed an increase in expression of ARHGAP18 under oxidative stress or after tumor necrosis factor-α stimulation.[19] Together with our findings herein, in which ARHGAP18 is upregulated in ECs placed under flow-induced stress conditions, we suggest that ARHGAP18 may be a gene that is vital for survival and is upregulated as a protective mechanism in response to stress.

ARHGAP18 Depletion Alters the Inflammatory Status of the Endothelium

Alignment of cells under high shear laminar flow inhibits the expression of proinflammatory genes and inhibits the activation of the transcription factor, NF-κB.[33] Control or

ARHGAP18-depleted cells were placed under high shear laminar flow (20 dynes/cm^2) for 1 or 24 hours, and the localization of p65 (as a measure of NF-κB activation) was assessed. The p65 subunit of NF-κB transiently moved into the nucleus on initiation of flow, consistent with reported studies[34] in both the control and ARHGAP18 siRNA-transfected cells (Figure 4Aiii, iv). After 24 hours of high shear laminar flow, p65 in the small-interfering control–transfected cells was predominantly relocalized to the cytoplasm (Figure 4Av). In contrast, a significant number of ARHGAP18-depleted cells (62±17 versus 12±4) have p65 retained in the nucleus (Figure 4Avi, white arrows, and quantified in Figure 4Avii). Thus, in the absence of ARHGAP18, even under high shear laminar flow, the ECs display an activated phenotype in contrast to normal cells under similar conditions. Although p65 underwent cytoplasmic-to-nuclear shuttling, ARHGAP18 did not undergo any changes in localization (Figure S3i–vi); however, there was a reduction in the total amount of ARHGAP18 in these cells subjected to high shear laminar flow for 24 hours, as previously seen for 72-hour high shear laminar flow (Figure 1).

We performed en face staining of *Arhgap18*$^{-/-}$ mice, focusing specifically on the endothelial layer, using confocal imaging techniques. This revealed an enhanced p65 expression in the endothelium in the athero-prone region (arches) of the *Arhgap18*$^{-/-}$ mice (Figure 4Bii) compared with WT controls (Figure 4Bi). Although the increased level of NF-κB was predominantly cytoplasmic (inactive), many cells also showed nuclear localization (highlighted in red) consistent with activated NF-κB, suggesting that the cells may be "primed," as has been reported by Passerini et al.[35] However, most striking was the extent and level of expression of NF-κB in the thoracic aorta regions in the *Arhgap18*$^{-/-}$ mice (Figure 4Biv) compared with WT (Figure 4Biii), showing predominantly cytoplasmic but also some nuclear localization in the *Arhgap18*$^{-/-}$ mice.

The number of NF-κB–positive ECs was quantified in aortic arch (WT versus *Arhgap18*$^{-/-}$, 37.1±8.3 versus 61.8±5.7) and the thoracic aorta (23.9±5.8 versus 42.1±11.8) (Figure 4Bv). Enhanced expression of ICAM-1 was also seen in the arches and to a more variable extent in the thoracic regions in the *Arhgap18*$^{-/-}$ mice compared with WT (9.3±9 versus 31±11) (Figure 4Cv). Analysis of eNOS, a vessel stabilizer, consistently showed a small but significantly reduced expression both in the arch (74.1±3.7 versus 69.1±2.2) and in the thoracic aorta (72.9±3 versus 68.4±1.4) regions of the *Arhgap18*$^{-/-}$ mice (Figure 4D). Together, the in vivo and in vitro data demonstrate that in the absence of *Arhgap18*, both proinflammatory and anti-inflammatory proteins in the endothelium are altered, priming the endothelium toward a proinflammatory phenotype, a situation
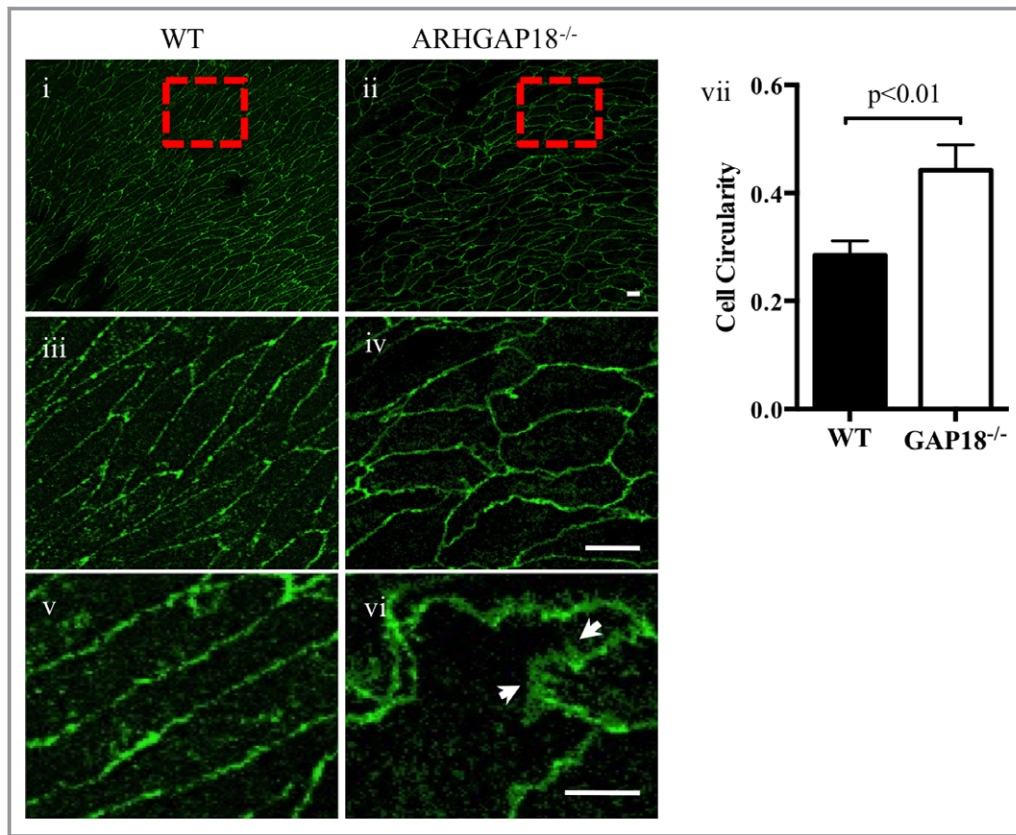
Figure 3. ARHGAP18 is flow responsive. En face view of the thoracic aorta stained for VE-cadherin (green) in high shear area of wild-type (WT; i, iii, and v) and *Arhgap18*$^{-/-}$ (ii, iv, and vi) mice. Magnified images of WT (iii and v) and *Arhgap18*$^{-/-}$ (iv and vi) mice correspond to boxed areas in i and ii, respectively. Cell elongation is measured using the formula for circularity, which is 4p (area/perimeter squared). A value of 1 indicates a perfect circle, and values approaching 0 indicate an oblong (noncircular) shape. (vii) Quantifications of 5 images taken from similar areas of the thoracic aorta from 5 different mice/group (0.28±0.02 vs 0.44±0.04, WT versus GAP18$^{-/-}$). Data are expressed as mean±SD. Bar=10 µm.

that we predict is exacerbated with further stress, such as an HFD.

ApoE$^{-/-}$/*Arhgap18*$^{-/-}$ DKO Mice Have Widespread Atherosclerosis

To determine whether *Arhgap18* deficiency affects atherosclerosis development, the *Arhgap18*$^{-/-}$ mice were fed a HFD, but there was no atherosclerosis evident (data not shown). These mice were then crossed with the athero-prone ApoE$^{-/-}$ mice to generate the DKO ApoE$^{-/-}$/*Arhgap18*$^{-/-}$. Male mice were fed a HFD for 4 to 20 weeks. Atherosclerotic plaques were identified by oil red O stain. After 8 weeks on the HFD, small atherosclerotic plaques were seen in the arches and in the arterial branches of both ApoE$^{-/-}$ and DKO, and there was a slight but not significant increase in lesions in the DKO (Figure 5Ai). After 20 weeks on HFD, atherosclerotic plaques were seen in the aortic arch, including near the brachiocephalic, left common carotid and left subclavian artery, but considerably

larger atherosclerotic plaques were seen in these regions in the DKO mice (Figure 5Aii). However, strikingly, there was a significant increase in the number of lesions in the thoracic aorta in the DKO mice. Lesions in the arch (ApoE$^{-/-}$ versus DKO, 7.4±1.3 versus 8.3±1.1) compared with lesions along the thoracic aorta (7.6±4.1 versus 14±5) (Figure 5Aii, iii), a region protected from atherosclerosis development with usually only minimal plaque development, were seen at the vessel branch points, as seen in the ApoE$^{-/-}$ mice. Hematoxylin and eosin staining of the 20-week atherosclerotic lesions in both the ascending aorta (Figure 5Bi and ii) and the aortic root area (Figure 5Ci and ii) showed more aggressive plaque formation in the DKO mice compared with ApoE$^{-/-}$ mice. Quantification of lesion size revealed a significantly larger total plaque area and thicker intimal layer, with slightly thinner medial layer, in DKO compared with ApoE$^{-/-}$ mice in both the ascending aorta (ApoE$^{-/-}$ versus DKO, 0.42±0.02 versus 0.76±0.16 and 0.17±0.03 versus 0.27±0.02, respectively) (Figure 5Biii and iv) and the aortic roots (ApoE$^{-/-}$ versus DKO, 0.73±0.2 versus
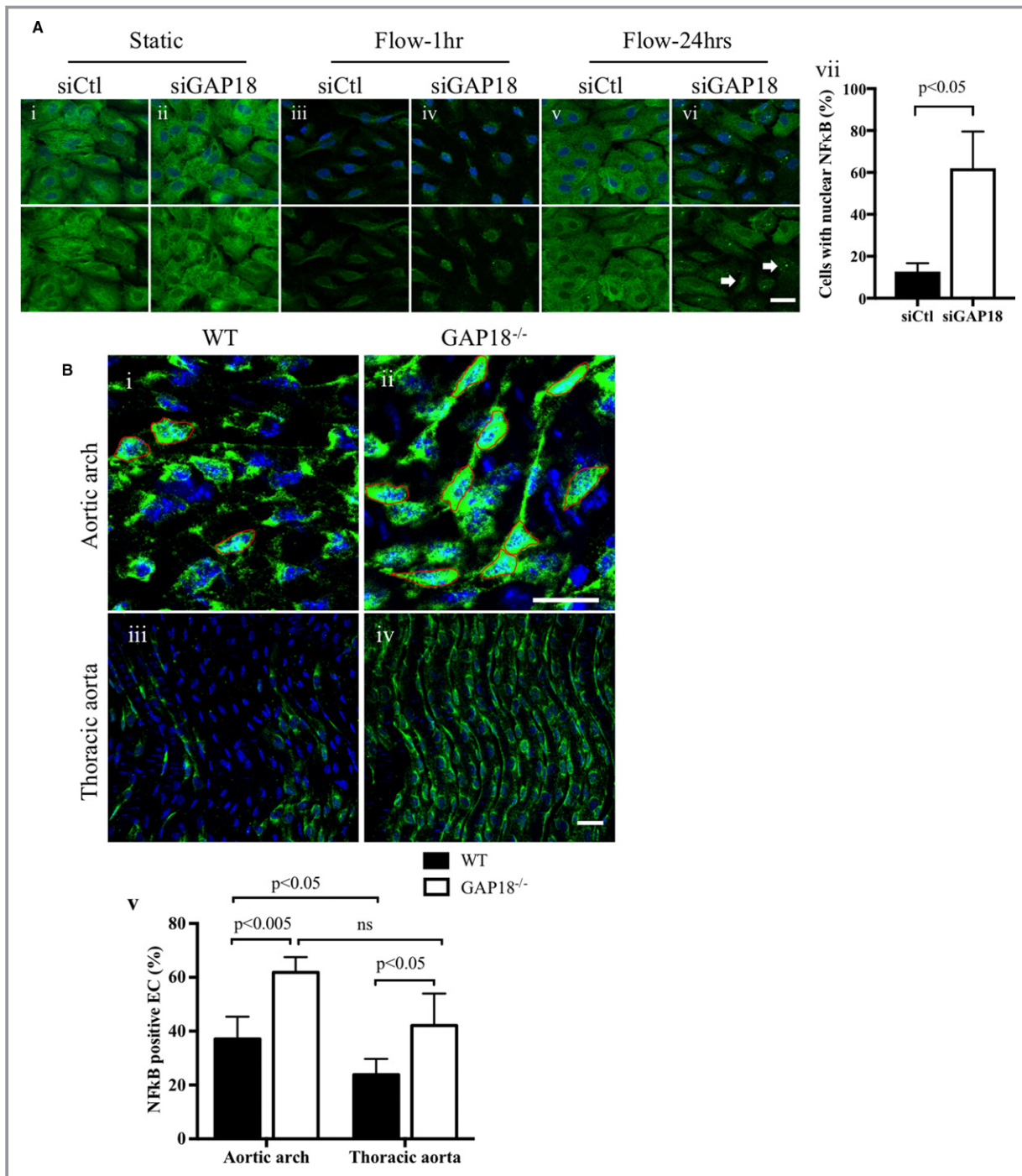
Figure 4. Loss of *Arhgap18* renders endothelial cells (ECs) proinflammatory. (**A**) Retention of nuclear factor-κB (NF-κB; p65) in ARHGAP18-deficient ECs. Control small-interfering RNA (siCtl; i, iii and v) or small-interfering ARHGAP18 (siGAP18)–treated ECs (ii, iv, and vi) under static condition (i and ii) and under 1-hour (iii and iv) and 24-hour high shear laminar flow (v and vi). NF-κB (p65), green; nuclei, blue. Representative images of 3 independent experiments. (vii) Quantification of NF-κB activation was determined by counting the number of cells with nuclear p65 per image field. Approximately 3000 total cells were counted from of 3 biological replicates. $P<0.05$. (**B**) Expression of the NF-κB (green) in the endothelium of wild-type (WT; i and iii) and *Arhgap18*$^{-/-}$ (GAP18$^{-/-}$) (ii and iv) mice with quantification of NF-κB–positive ECs in the aortic arch (37.1 ± 8.3 vs 61.8 ± 5.7, WT vs GAP18$^{-/-}$) and the thoracic aorta regions (23.9 ± 5.8 vs 42.1 ± 11.8, WT versus GAP18$^{-/-}$) (v). (**C**) Intercellular adhesion molecule 1 (ICAM-1) expression in the aorta in WT (i and iii) and GAP18$^{-/-}$ (ii and iv) mice with quantification of ICAM-1–positive ECs (9.3 ± 9 vs 31 ± 11, WT versus GAP18$^{-/-}$) (v). (**D**) Quantification of endothelial nitric oxide synthase (eNOS; red) expression in ECs from WT and GAP18$^{-/-}$ mice in the aortic arch (74.1 ± 3.7 vs 69.1 ± 2.2, WT versus GAP18$^{-/-}$) and the thoracic aorta regions (72.9 ± 3 vs 68.4 ± 1.4, WT versus GAP18$^{-/-}$). Images and quantifications are representative of 3 independent experiments. Nuclei, blue. Bar=25 µm. Ns indicates not significant.
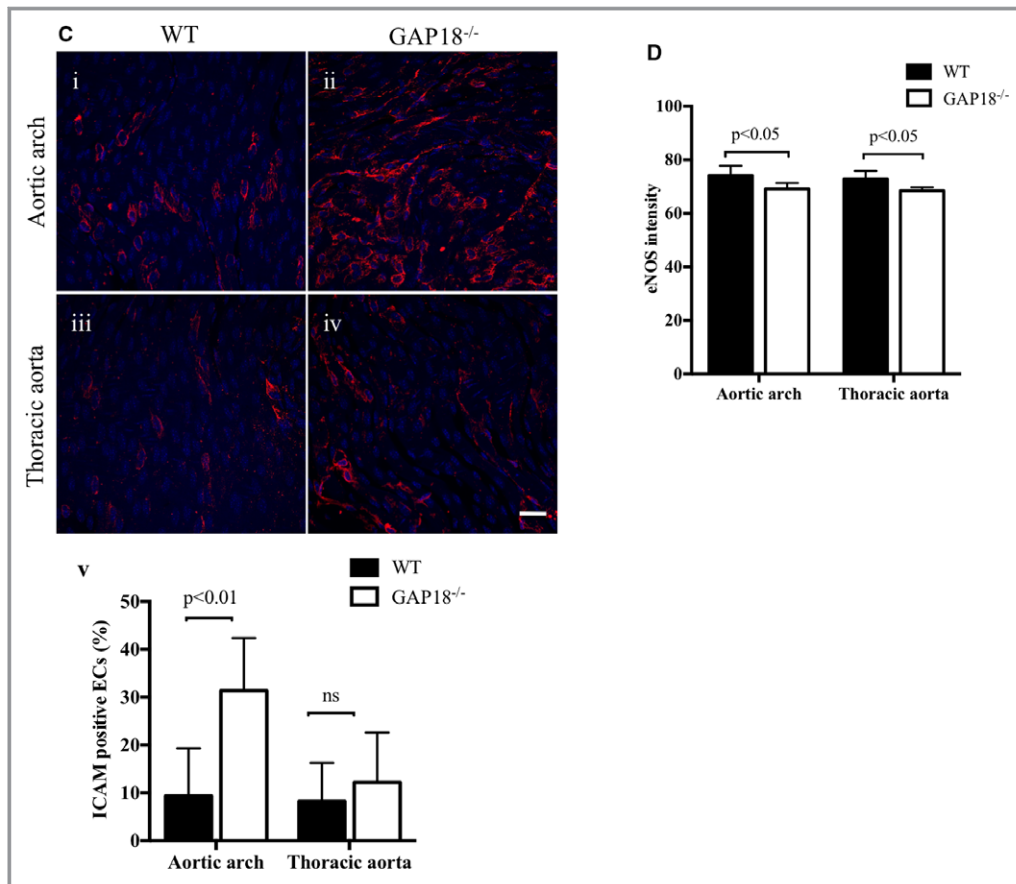
Figure 4. Continued

1.6±0.2 and 0.2±0.03 versus 0.33±0.05, respectively) (Figure 5Ciii–iv).

ARHGAP18 Deletion Promotes Early Onset of Atherosclerosis

The DKO mice showed early onset of atherosclerosis. After 4 weeks on the HFD, a thin layer of fatty streak without inflammatory infiltrates was observed in ApoE$^{-/-}$ mice (blue bar in Figure 6Ai). In contrast, the DKO mice showed a much thicker layer of fatty streak accompanied by high numbers of morphologically large vacuolated cells, which are likely macrophage foam cells (Figure 6Aii). By 8 weeks, the fatty streak in ApoE$^{-/-}$ mice had increased in thickness, accompanied by some degree of inflammatory cell infiltration (Figure 6Aiii). However, the lesions in the DKO mice at 8 weeks of HFD were significantly more advanced, as evidenced by the presentation of cholesterol clefts (Figure 6Aiv, yellow arrows) and macrophage foam cells (Figure 6Aiv, green arrowheads). Furthermore, there was increased infiltration of CD45-positive lymphocytes within the plaque in the DKO mice (Figure 6Bii and iv) compared with ApoE$^{-/-}$ mice (Figure 6Bi and iii) at both 4 and 8 weeks of HFD.

ARHGAP18 Deletion Does Not Affect Lipid Metabolism in ApoE$^{-/-}$ Mice

Altered lipid metabolism is a key factor in the onset and progression of atherosclerosis. To determine whether ARHGAP18 deficiency modulates lipid metabolism to promote atherosclerosis, we compared the lipid profiles in the mutant mice. DKO and ApoE$^{-/-}$ mice, age and sex matched, have comparable body weight under normal diet and HFD challenged (Figure S4A). Plasma levels of total triglyceride and total cholesterol, including the high- and low-density lipoproteins, were not different between the ApoE$^{-/-}$ and DKO mice (Figure S4B), suggesting that ARHGAP18 deficiency did not alter lipid metabolism.

Discussion

Cell alignment in the direction of flow is a major protective response of ECs to shear stress. The alignment and remodeling is mediated through the dynamic regulation of the family of Rho GTPases.[30] Herein, we demonstrate that ARHGAP18 (aka, *SENEX*),[19] a negative regulator of Rho,[19,22] is flow responsive and is essential for the alignment of ECs in the
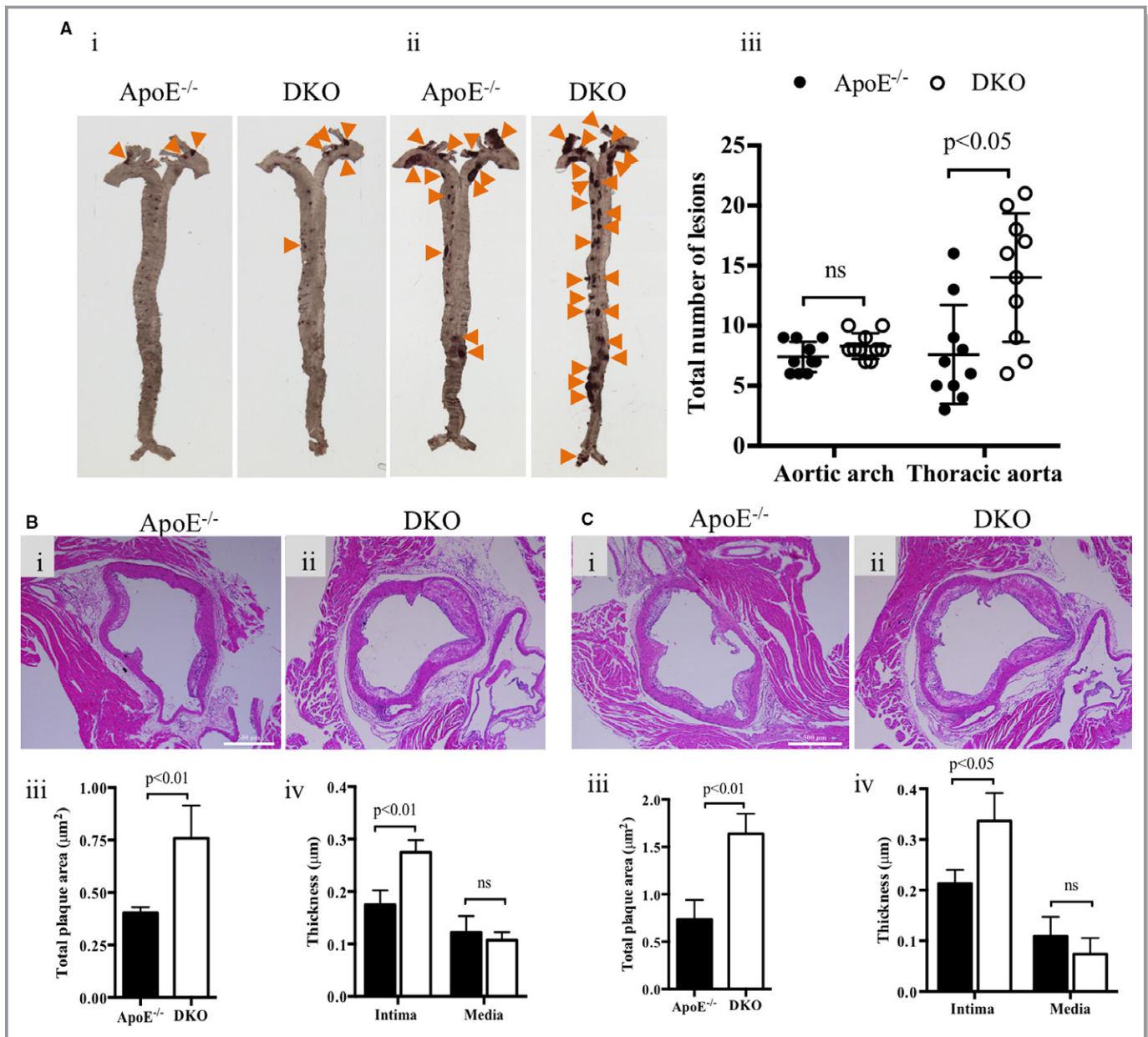
Figure 5. Enhanced atherosclerosis in *Arhgap18*-deficient mice. (**A**) Apolipoprotein E (ApoE)$^{-/-}$ and ApoE/*Arhgap18* double-knockout (DKO) mice were fed a high-fat diet for 8 (i) and 20 (ii) weeks, respectively. The presence of atherosclerotic lesions (arrows) along the aortic tree was detected by en face staining with Oil Red O. Representative images of 10 mice are shown. Total number of lesions in the aortic arch and along the aortic tree were counted. Lesion in the aortic arch includes near the brachiocephalic trunk, left common carotid artery, and the left subclavian artery. Lesions in the thoracic aorta cover areas from the ligamentum arteriosum extending distally to the iliac bifurcation. (iii) Total lesions counted in the arch (ApoE$^{-/-}$ vs DKO, 7.4±1.3 vs 8.3±1.1) and along the thoracic aorta (7.6±4.1 vs 14±5). Data are expressed as mean±SD. Statistical analysis was made by 2-tailed unpaired Student *t* test unless stated otherwise. *P*<0.05 was considered significant, n=5 mice per group. (**B**) (i, ii) Hematoxylin and eosin (H&E) stain showing atherosclerotic lesions in cross sections of the ascending aorta after 20 weeks of high-fat diet. Representative images of 5 mice/group are shown. Total plaque area was normalized to total area of the aorta (ApoE$^{-/-}$ vs DKO, 0.42±0.02 vs 0.76±0.16) (iii) and intimal thickness measurement (ApoE$^{-/-}$ vs DKO, 0.17±0.03 vs 0.27±0.02) (iv). n=5 mice/group. (**C**) H&E stain of advanced atherosclerotic lesions found in areas of the aortic roots in ApoE$^{-/-}$ (i) and DKO (ii) mice. Representative images of 5 mice/group are shown. Quantification of the total plaque area in aortic root (ApoE$^{-/-}$ vs DKO, 0.73±0.2 vs 1.6±0.2) (iii) and in the media (ApoE$^{-/-}$ vs DKO, 0.2±0.03 vs 0.33±0.05) (iv). Data are expressed as mean±SD. *P*<0.05 by 2-tailed unpaired Student *t* test. n=5 mice per group.
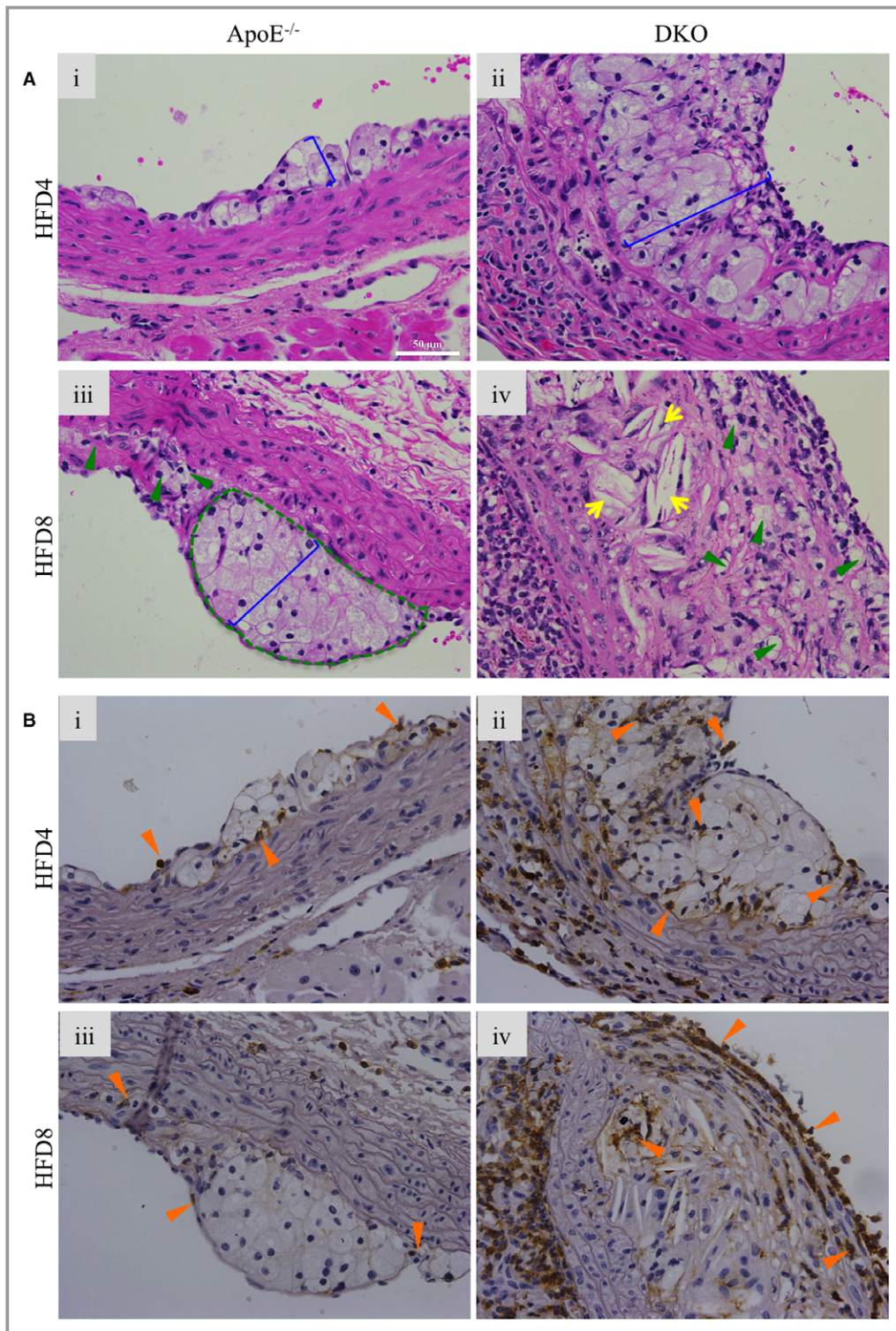
Figure 6. Deletion of ARHGAP18 promotes early onset of atherosclerosis. (**A**) Hematoxylin and eosin staining of cross sections of the ascending aorta after 4 weeks (i and ii) or 8 weeks (iii and iv) on a high-fat diet (HFD). The thickness of atherosclerotic lesions is shown with the blue line. Cholesterol clefts (yellow arrows) and a cluster of foam cells or fatty streaks (green circled) and their presence within the atherosclerotic plaque (green arrows) are indicated. (**B**) CD45-positive lymphocytes infiltrate (orange arrows) in apolipoprotein E (ApoE)$^{-/-}$ and double-knockout (DKO) mice after 4 weeks (i and ii) and 8 weeks (iii and iv) of HFD. Representative images from 5 mice/group.

direction of flow. Loss of *Arhgap18* impairs EC alignment, primes the endothelium toward a proinflammatory phenotype, and accelerates the development of HFD-induced atherosclerosis. Together with our previous work showing ARHGAP18 being essential for EC survival[19] and as an inhibitor of angiogenesis,[22] our data suggest that ARHGAP18 is a vascular protective gene.

The *Arhgap18*^{−/−} mice exhibit 2 unusual phenotypes in the descending thoracic aorta. First, they show high atherosclerosis plaque development, in a region normally associated with atheroprotection. Second, they have impaired EC alignment in the direction of flow, and staining for the junctional protein, VE-cadherin, showed a disrupted phenotype. The lack of alignment of the ECs is consistent with the well-accepted concept that the alignment is necessary to maintain the anti-inflammatory and quiescent phenotype of the endothelium that is resistant to atherosclerosis.[29,36,37] Indeed, our imaging data, in which the focus is on expression of those proteins specifically only in the EC layer, show an alteration in the inflammatory nature of the endothelium in the *Arhgap18*^{−/−} mice. The inflammatory nature of the endothelium is known to be an early and key event in atherosclerosis initiation and development.[4] In the descending thoracic aorta of *Arhgap18*^{−/−} mice, there was a significant increase in the expression of the proinflammatory transcriptional factor, NF-κB, and the proinflammatory protein, ICAM-1, and a decrease in the anti-inflammatory protein, eNOS. Thus, the upregulation of the proinflammatory and downregulation of the anti-inflammatory markers would suggest that the ECs are primed for inflammation and that this priming together with a risk factor, such as an HFD, accelerate and enhance atherosclerosis development.

The dynamic nature of the Rho GTPase cycle is critical in EC alignment to shear stress because both constitutively activated and inactivated Rho impairs this alignment process.[30,38] Although there are many GAP proteins that may inhibit Rho signaling, our data show that *Arhgap18* is critical in the alignment process because its depletion, either in vitro or in vivo, results in a failure of ECs to align in response to high shear stress. The lack of microtubule-organizing center reorganization on *ARHGAP18* depletion suggests its importance in the early events in the alignment process. We have previously shown that ARHGAP18 acts to regulate the activity of the RhoC-ROCK (Rho-associated protein kinase) pathway in ECs, with no effect on RhoA.[22] Thus, ARHGAP18 demonstrates cell type selectivity for Rho because in ECs, it has RhoC activity, whereas in non-ECs, it has RhoA activity.[23] As with RhoA, RhoC is also important in cytoskeletal dynamics. Loss of RhoC results in an accumulation of thick actin bundles in the protruding edge of cells[39] and an increase in EC migration.[40] *Arhgap18* depletion in ECs, where RhoC activation is enhanced and maintained, results in a disruption of the actin cytoskeleton and a loss of cell junctional integrity[22]; and herein we show

a failure of the cells to reorganize in the direction of flow. Thus, our data would suggest that RhoC is also critical in the alignment process and in EC homeostasis. Another RhoGAP, p190RhoGAP, has been implicated in the activation phase of RhoA in response to shear stress,[38] suggesting that multiple RhoGAPs are thus likely to be coordinated to "fine-tune" the EC response to flow. Recently, we have localized ARHGAP18 to the microtubules, its expression being essential for microtubule stability and for microtubule-dependent functions in ECs.[41] The cytoskeleton and, in particular, microtubules are also known to influence NF-κB activation, a key regulator of inflammatory genes.[42,43] Furthermore, Rho GTPases interact with the NF-κB pathway and can exert either positive or negative signals on its activation, depending on the milieu and activation.[44–46] Our results in vitro show depletion of *Arhgap18*, resulting in a lack of EC alignment, leads to a sustained nuclear localization of the p65 subunit of NF-κB, even under high shear stress. The results are confirmed in the thoracic and arch regions of *Arhgap18*^{−/−} mice, where there is an increase in both total p65 and its nuclear localization. Thus, loss of *Arhgap18* predisposes the ECs toward the inflammatory state.

To date, many genes have been implicated in the flow-mediated alignment process of ECs. Interestingly, Sydecan-4[29] is also protective against vascular diseases, such as atherosclerosis. Syndecan-4, among other functions, regulates the small GTPases, Rac1, RhoA, and RhoG.[47] ROCK is a downstream effector of the small Rho GTPases (including RhoC), and high ROCK activity is associated with areas of vessel stiffness,[48] regions prone to enhanced leukocyte adhesion and EC permeability[49] and to the development of cardiovascular disease.[50] Thus, treating cardiovascular disease through targeting Rho activity has been proposed, and the ROCK inhibitor fasudil has shown some benefit, at least in pulmonary hypertensive patients.[51] The identification of the Rho GTPase inhibitor, ARHGAP18, as a critical regulator of the protective alignment process supports such an approach.

Acknowledgments

Author Contributions

Lay devised the study, performed experiments, interpreted data, and wrote the manuscript. Preston, Coleman, and Ting performed different aspects of experiments. Roediger and Weninger collaborated in the analysis of the knockout mice.
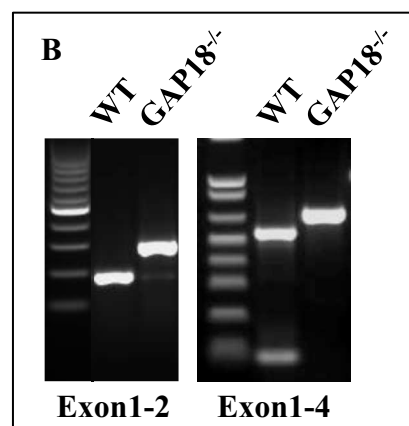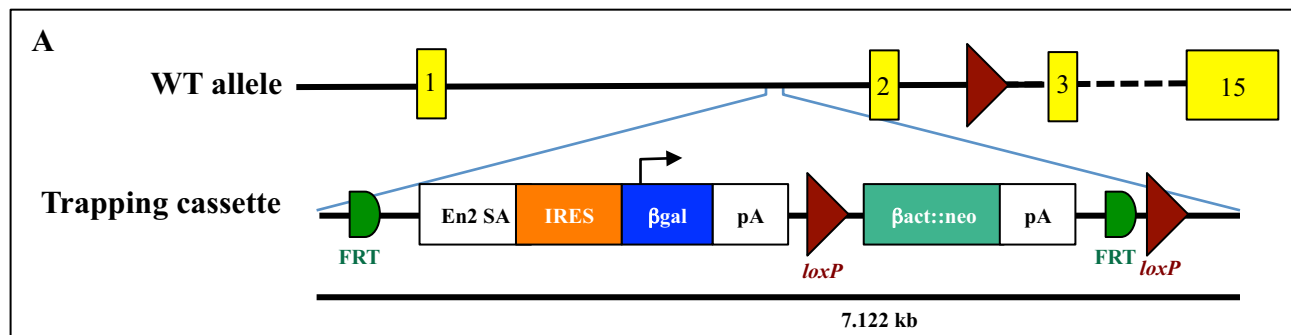
References

1. Conway DE, Breckenridge MT, Hinde E, Gratton E, Chen CS, Schwartz MA. Fluid shear stress on endothelial cells modulates mechanical tension across VE-cadherin and PECAM-1. *Curr Biol*. 2013;23:1024–1030.

2. Libby P, Bornfeldt KE, Tall AR. Atherosclerosis: successes, surprises, and future challenges. *Circ Res*. 2016;118:531–534.

3. Lusis AJ. Atherosclerosis. *Nature*. 2000;407:233–241.

4. Heusch G, Libby P, Gersh B, Yellon D, Bohm M, Lopaschuk G, Opie L. Cardiovascular remodelling in coronary artery disease and heart failure. *Lancet*. 2014;383:1933–1943.

5. Gimbrone MA Jr, García-Cardeña G. Vascular endothelium, hemodynamics, and the pathobiology of atherosclerosis. *Cardiovasc Pathol*. 2013;22:9–15.

6. Davies PF. Hemodynamic shear stress and the endothelium in cardiovascular pathophysiology. *Nat Clin Pract Cardiovasc Med*. 2009;6:16–26.

7. Chiu JJ, Chien S. Effects of disturbed flow on vascular endothelium: pathophysiological basis and clinical perspectives. *Physiol Rev*. 2011;91:327–387.

8. Davies PF, Civelek M, Fang Y, Fleming I. The atherosusceptible endothelium: endothelial phenotypes in complex haemodynamic shear stress regions in vivo. *Cardiovasc Res*. 2013;99:315–327.

9. Conway DE, Schwartz MA. Flow-dependent cellular mechanotransduction in atherosclerosis. *J Cell Sci*. 2013;126:5101–5109.

10. Won D, Zhu SN, Chen M, Teichert AM, Fish JE, Matouk CC, Bonert M, Ojha M, Marsden PA, Cybulsky MI. Relative reduction of endothelial nitric-oxide synthase expression and transcription in atherosclerosis-prone regions of the mouse aorta and in an in vitro model of disturbed flow. *Am J Pathol*. 2007;171:1691–1704.

11. Huddleson JP, Ahmad N, Srinivasan S, Lingrel JB. Induction of KLF2 by fluid shear stress requires a novel promoter element activated by a phosphatidylinositol 3-kinase-dependent chromatin-remodeling pathway. *J Biol Chem*. 2005;280:23371–23379.

12. Dekker RJ, van Soest S, Fontijn RD, Salamanca S, de Groot PG, VanBavel E, Pannekoek H, Horrevoets AJ. Prolonged fluid shear stress induces a distinct set of endothelial cell genes, most specifically lung Kruppel-like factor (KLF2). *Blood*. 2002;100:1689–1698.

13. Hamik A, Lin Z, Kumar A, Balcells M, Sinha S, Katz J, Feinberg MW, Gerzsten RE, Edelman ER, Jain MK. KRUPPEL-like factor 4 regulates endothelial inflammation. *J Biol Chem*. 2007;282:13769–13779.

14. Conway D, Schwartz MA. Lessons from the endothelial junctional mechanosensory complex. *F1000 Biol Rep*. 2012;4:1.

15. Wojciak-Stothard B, Ridley AJ. Shear stress-induced endothelial cell polarization is mediated by Rho and Rac but not Cdc42 or PI 3-kinases. *J Cell Biol*. 2003;161:429–439.

16. Cherfils J, Zeghouf M. Regulation of small GTPases by GEFs, GAPs, and GDIs. *Physiol Rev*. 2013;93:269–309.

17. Moon SY, Zheng Y. Rho GTPase-activating proteins in cell regulation. *Trends Cell Biol*. 2003;13:13–22.

18. Neisch AL, Formstecher E, Fehon RG. Conundrum, an ARHGAP18 orthologue, regulates RhoA and proliferation through interactions with Moesin. *Mol Biol Cell*. 2013;24:1420–1433.

19. Coleman PR, Hahn CN, Grimshaw M, Lu Y, Li X, Brautigan PJ, Beck K, Stocker R, Vadas MA, Gamble JR. Stress-induced premature senescence mediated by a novel gene, senex, results in an anti-inflammatory phenotype in endothelial cells. *Blood*. 2010;116:4016–4024.

20. Coleman PR, Chang G, Hutas G, Grimshaw M, Vadas MA, Gamble JR. Age-associated stresses induce an anti-inflammatory senescent phenotype in endothelial cells. *Aging (Albany NY)*. 2013;5:913–924.

21. Powter EE, Coleman PR, Tran MH, Lay AJ, Bertolino P, Parton RG, Vadas MA, Gamble JR. Caveolae control the anti-inflammatory phenotype of senescent endothelial cells. *Aging Cell*. 2015;14:102–111.

22. Chang GH, Lay AJ, Ting KK, Zhao Y, Coleman PR, Powter EE, Formaz-Preston A, Jolly CJ, Bower NI, Hogan BM, Rinkwitz S, Becker TS, Vadas MA, Gamble JR. ARHGAP18: an endogenous inhibitor of angiogenesis, limiting tip formation and stabilizing junctions. *Small GTPases*. 2014;5:1–15.

23. Maeda M, Hasegawa H, Hyodo T, Ito S, Asano E, Yuang H, Funasaka K, Shimokata K, Hasegawa Y, Hamaguchi M, Senga T. ARHGAP18, a GTPase-activating protein for RhoA, controls cell shape, spreading, and motility. *Mol Biol Cell*. 2011;22:3840–3852.

24. Liu R, Lo L, Lay AJ, Zhao Y, Ting KK, Robertson EN, Sherrah AG, Jarrah S, Li H, Zhou Z, Hambly BD, Richmond DR, Jeremy RW, Bannon PG, Vadas MA, Gamble JR. ARHGAP18 protects against thoracic aortic aneurysm formation by mitigating the synthetic and proinflammatory smooth muscle cell phenotype. *Circ Res*. 2017;121:512–524.

25. DuFort CC, Paszek MJ, Weaver VM. Balancing forces: architectural control of mechanotransduction. *Nat Rev Mol Cell Biol*. 2011;12:308–319.

26. Etienne-Manneville S. Actin and microtubules in cell motility: which one is in control? *Traffic*. 2004;5:470–477.

27. Litwin M, Clark K, Noack L, Furze J, Berndt M, Albelda S, Vadas M, Gamble J. Novel cytokine-independent induction of endothelial adhesion molecules regulated by platelet/endothelial cell adhesion molecule (CD31). *J Cell Biol*. 1997;139:219–228.

28. Pfaffl MW. A new mathematical model for relative quantification in real-time RT-PCR. *Nucleic Acids Res*. 2001;29:e45.

29. Baeyens N, Mulligan-Kehoe MJ, Corti F, Simon DD, Ross TD, Rhodes JM, Wang TZ, Mejean CO, Simons M, Humphrey J, Schwartz MA. Syndecan 4 is required for endothelial alignment in flow and atheroprotective signaling. *Proc Natl Acad Sci USA*. 2014;111:17308–17313.

30. Tzima E, del Pozo MA, Shattil SJ, Chien S, Schwartz MA. Activation of integrins in endothelial cells by fluid shear stress mediates Rho-dependent cytoskeletal alignment. *EMBO J*. 2001;20:4639–4647.

31. Tzima E, Kiosses WB, del Pozo MA, Schwartz MA. Localized cdc42 activation, detected using a novel assay, mediates microtubule organizing center positioning in endothelial cells in response to fluid shear stress. *J Biol Chem*. 2003;278:31020–31023.

32. Giannotta M, Trani M, Dejana E. VE-cadherin and endothelial adherens junctions: active guardians of vascular integrity. *Dev Cell*. 2013;26:441–454.

33. Topper JN, Gimbrone MA Jr. Blood flow and vascular gene expression: fluid shear stress as a modulator of endothelial phenotype. *Mol Med Today*. 1999;5:40–46.

34. Orr AW, Sanders JM, Bevard M, Coleman E, Sarembock IJ, Schwartz MA. The subendothelial extracellular matrix modulates NF-kappaB activation by flow: a potential role in atherosclerosis. *J Cell Biol*. 2005;169:191–202.

35. Passerini AG, Polacek DC, Shi C, Francesco NM, Manduchi E, Grant GR, Pritchard WF, Powell S, Chang GY, Stoeckert CJ Jr, Davies PF. Coexisting proinflammatory and antioxidative endothelial transcription profiles in a disturbed flow region of the adult porcine aorta. *Proc Natl Acad Sci USA*. 2004;101:2482–2487.

36. Traub O, Berk BC. Laminar shear stress: mechanisms by which endothelial cells transduce an atheroprotective force. *Arterioscler Thromb Vasc Biol*. 1998;18:677–685.

37. Wang C, Baker BM, Chen CS, Schwartz MA. Endothelial cell sensing of flow direction. *Arterioscler Thromb Vasc Biol*. 2013;33:2130–2136.

38. Yang B, Radel C, Hughes D, Kelemen S, Rizzo V. P190 rhogtpase-activating protein links the beta1 integrin/caveolin-1 mechanosignaling complex to RhoA and actin remodeling. *Arterioscler Thromb Vasc Biol*. 2011;31:376–383.

39. Mitin N, Rossman KL, Currin R, Anne S, Marshall TW, Bear JE, Bautch VL, Der CJ. The rhoGEF TEM4 regulates endothelial cell migration by suppressing actomyosin contractility. *PLoS One*. 2013;8:e66260.

40. Hoeppner LH, Sinha S, Wang Y, Bhattacharya R, Dutta S, Gong X, Bedell VM, Suresh S, Chun C, Ramchandran R, Ekker SC, Mukhopadhyay D. RhoC maintains vascular homeostasis by regulating VEGF-induced signaling in endothelial cells. *J Cell Sci*. 2015;128:3556–3568.

41. Lovelace MD, Powter EE, Coleman PR, Zhao Y, Parker A, Chang GH, Lay AJ, Hunter J, McGrath AP, Jormakka M, Bertolino P, McCaughan G, Kavallaris M, Vadas MA, Gamble JR. The RhoGAP protein ARHGAP18/SENEX localizes to microtubules and regulates their stability in endothelial cells. *Mol Biol Cell*. 2017;28:1066–1078.

42. Olson EN, Nordheim A. Linking actin dynamics and gene transcription to drive cellular motile functions. *Nat Rev Mol Cell Biol*. 2010;11:353–365.

43. Rosette C, Karin M. Cytoskeletal control of gene expression: depolymerization of microtubules activates NF-kappa B. *J Cell Biol*. 1995;128:1111–1119.

44. Fritz G, Kaina B. Ras-related GTpase Rhob represses NF-kappaB signaling. *J Biol Chem*. 2001;276:3115–3122.

45. Montaner S, Perona R, Saniger L, Lacal JC. Multiple signalling pathways lead to the activation of the nuclear factor kappaB by the Rho family of GTPases. *J Biol Chem*. 1998;273:12779–12785.

46. Tong L, Tergaonkar V. Rho protein GTPases and their interactions with NFkappaB: crossroads of inflammation and matrix biology. *Biosci Rep*. 2014;34:e00115.

47. Brooks R, Williamson R, Bass M. Syndecan-4 independently regulates multiple small GTPases to promote fibroblast migration during wound healing. *Small GTPases*. 2012;3:73–79.

48. Noma K, Goto C, Nishioka K, Jitsuiki D, Umemura T, Ueda K, Kimura M, Nakagawa K, Oshima T, Chayama K, Yoshizumi M, Liao JK, Higashi Y. Roles of Rho-associated kinase and oxidative stress in the pathogenesis of aortic stiffness. *J Am Coll Cardiol*. 2007;49:698–705.

49. Huynh J, Nishimura N, Rana K, Peloquin JM, Califano JP, Montague CR, King MR, Schaffer CB, Reinhart-King CA. Age-related intimal stiffening enhances endothelial permeability and leukocyte transmigration. *Sci Transl Med*. 2011;3:112ra122.

50. Hahn C, Schwartz MA. Mechanotransduction in vascular physiology and atherogenesis. *Nat Rev Mol Cell Biol*. 2009;10:53–62.

51. Surma M, Wei L, Shi J. Rho kinase as a therapeutic target in cardiovascular disease. *Future Cardiol*. 2011;7:657–671.
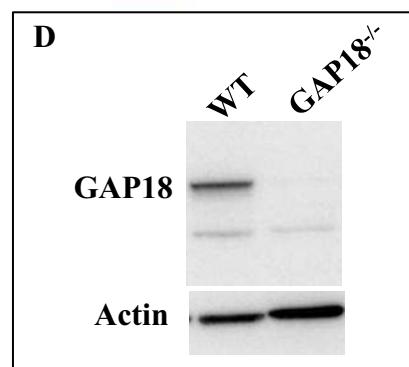
SUPPLEMENTAL MATERIAL

Figure S1A-D. Generation of ARHGAP18 knockout mice. **(A***)* Diagrammatic representation of the transgenic allelle containing trapping cassette SA-βgeo-pA (splice acceptor-beta-geo polyA) which then inserted into the intronic region immediately upstream of exon2. The 7.2 kb construct contains LacZ reporter gene flanked by Flp-recombinase target (FRT) sites. Through efficient splicing to the reporter cassette, a truncation of the endogenous transcript is generated resulting in the generation of a constitutive null mutation in the ARHGAP18 gene. **(B)** Homozygote mutant allele was identified using primers specific to exon 1-2 and 1-4. **(C)** Sequence analysis of PCR product from B showing integration of 115 nucleotide from the cassette in the ARHGAP18 mutant allele. **(D)** Western blot analysis of cultured bone marrow-derived macrophage from WT and ARHGAP18 knockout mice probed for ARHGAP18 (2A3-F3 mAb).
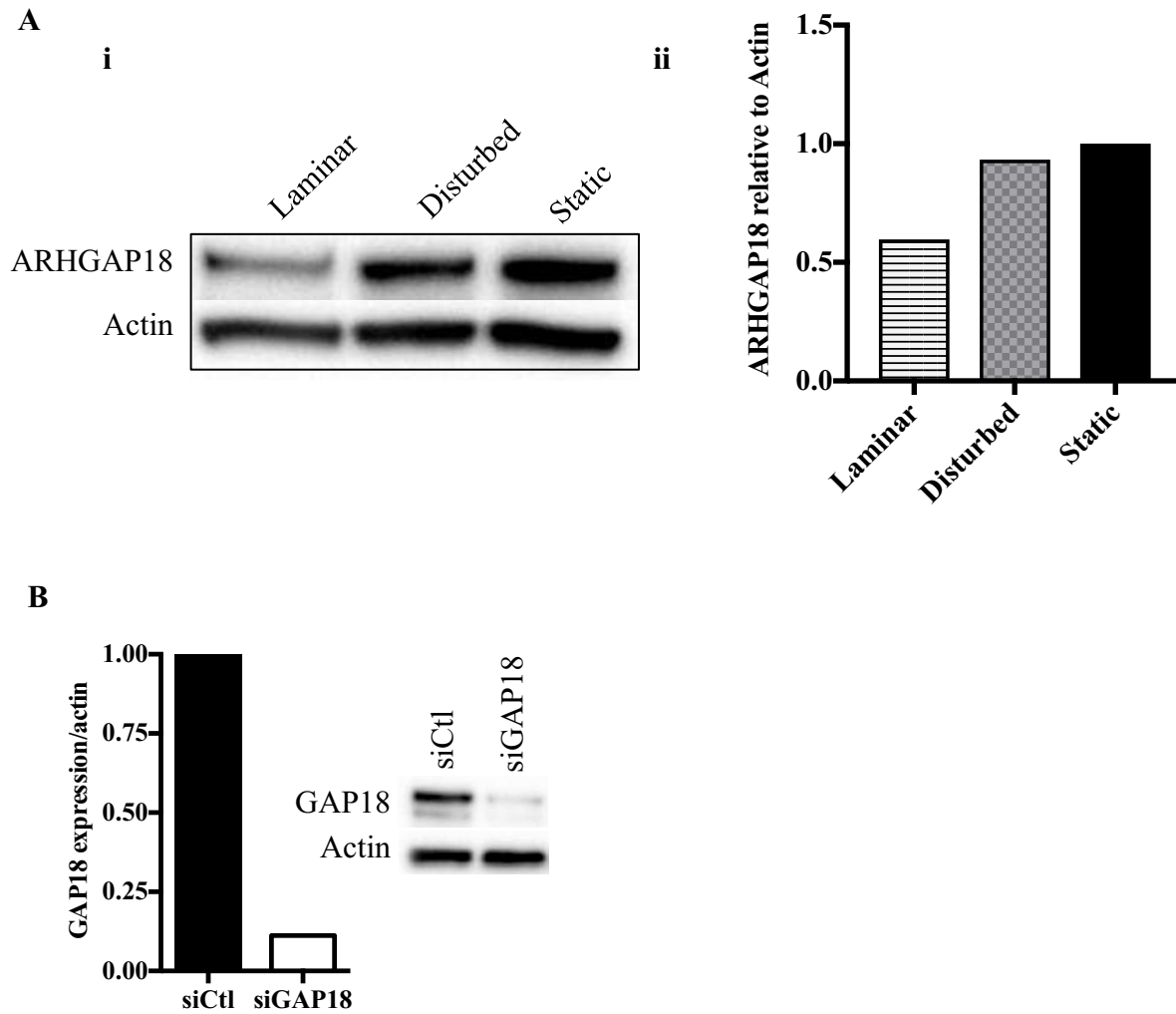
A

i

ii

B

***Figure S2A-B. ARHGAP18 regulation* (A)** *In vitro* analysis of ARHGAP18 protein expression in response to laminar flow, disturbed flow and under static conditions. **(B)** Densitometry quantification of Western blot in (A).

(B) A >90% reduction in ARHGAP18 mRNA expression level in HUVECs treated with siARHGAP18 (opened bar) compared to siControl (closed bar). Western blot analysis shows >90% knockdown of ARHGAP18 in siARHGAP18 treated cells compared to siControl.
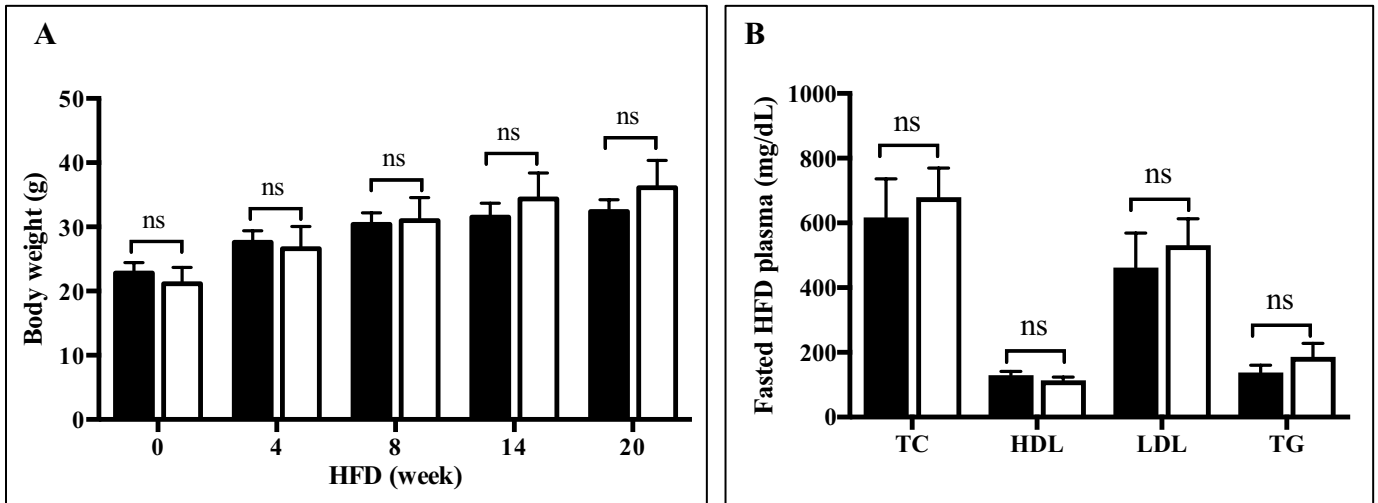
Figure S3A-B. Deletion in ARHGAP18 did not alter lipid profile in HFD mice. **(A***)* Body weight of ApoE (closed bar) or ApoE/ARHGAP18 double knockout (opened bar) mice at various time point post HFD treatment.   No significant differences in body weight were observed between the two genotypes at all time points. **(B)** Fasting blood level of total cholesterol (TC), High density lipoprotein (HDL), low density lipoprotein (LDL) and Triglycerides (TG) were not significantly different between ApoE and ApoE/ARHGA18 DKO.
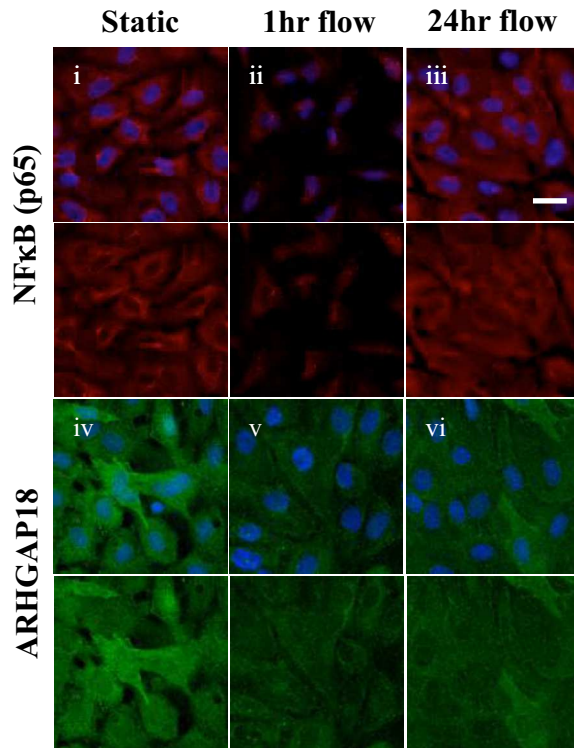
***Figure S4*. Flow stimulates NFκB (p65) localisation.**
Under static condition, NFkB (p65) resides in the cytoplasms. NFkB (p65) shuffle to the nucleus after 1 hour of laminar flow and returned to the cytoplasm after 24hr of laminar flow (i-iii). ARHGAP18 expression is down regulated under laminar flow at 1hr and 24 hr of laminar flow (iv-vi). NFkB (p65) (red), Nuclei (Blue) and ARHGAP18 (green). Representative images of 4 independent experiments.